

Evidence for oxygen-conserving diamond formation in redox-buffered subducted oceanic crust sampled as eclogite

Sonja Aulbach ¹✉ & Thomas Stachel²

Cratonic eclogite is the product of oceanic crust subduction into the subcontinental lithospheric mantle, and it also is a fertile diamond source rock. In contrast to matrix minerals in magma-borne xenoliths, inclusions in diamond are shielded from external fluids, retaining more pristine information on the state of the eclogite source at the time of encapsulation. Vanadium is a multi-valent element and a widely used elemental redox proxy. Here, we show that that xenolithic garnet has lower average V abundances than garnet inclusions. This partly reflects crystal-chemical controls, whereby higher average temperatures recorded by inclusions, accompanied by enhanced Na₂O and TiO₂ partitioning into garnet, facilitate V incorporation at the expense of clinopyroxene. Unexpectedly, although diamond formation is strongly linked to metasomatism and xenoliths remained open systems, V concentrations are similar for bulk eclogites reconstructed from inclusions and from xenoliths. This suggests an oxygen-conserving mechanism for eclogitic diamond formation, and implies that eclogite is an efficient system to buffer fO_2 over aeons of lithospheric mantle modification by subduction-derived and other fluids.

¹Institut für Geowissenschaften, Goethe-Universität, Frankfurt am Main, Germany. ²Earth and Atmospheric Sciences, University of Alberta, Edmonton, AB, Canada. ✉email: s.aulbach@em.uni-frankfurt.de

Oxygen fugacity (fO_2) is an intensive variable that controls the speciation and mobility of carbon and therefore its cycling among Earth's reservoirs¹; it is, therefore, often invoked to play a critical role in diamond formation^{2–4}. Kimberlite-borne eclogite xenoliths have protoliths that formed during partial melting of dry peridotite, probably at Mesoarchaean to Palaeoproterozoic spreading ridges, and can therefore provide invaluable information on the oxygen fugacity (fO_2) of the convecting mantle and the evolution of this parameter in deep time⁵. Like modern mid-ocean ridge basalts (MORB), the ancient protoliths underwent seawater alteration and metamorphism in subduction zones⁶, in part accompanied by diamond formation⁷. The compositions of isolated minerals entrapped in their chemically inert diamond host freeze-in concentrations that reflect temperatures and garnet-clinopyroxene equilibria at the time of diamond formation. In contrast, xenoliths continue to evolve via interaction with fluids and melt that cause mantle metasomatism⁸, giving rise to differences in the chemical composition of occluded minerals and their xenolithic counterparts⁹ (Fig. 1a). However, the diamond-forming process is itself already metasomatic in nature, and may have been accompanied by changes in chemical composition and possibly redox state^{3,10}.

Vanadium is a multi-valent element that becomes less compatible in mantle minerals with increasing fO_2 ^{11,12}, and is now widely applied as a redox proxy to unravel fO_2 attending the formation of mantle-derived melts and their residues^{11,13–15}. The development of the V redox proxy is particularly useful where conventional oxybarometry is difficult to apply, as in the case of isolated inclusions in a diamond. However, the simple mineralogy of xenolithic eclogites, composed of subequal proportions of garnet and clinopyroxene with a limited number of accessory minerals⁶, and their corresponding diamond source rocks at depth¹⁶, belies a complex evolution that would preclude a simple interpretation of mineral V abundances. Crystal-chemical controls on V incorporation in eclogite minerals are likely to play a role. This is important because inclusions in diamond (DI) are mostly unpaired (i.e., garnet or clinopyroxene only in a given eclogitic stone). Furthermore, apart from the redox-dependence of V partitioning, like any other trace element, V abundances in eclogite depend on accumulation-differentiation processes within the oceanic crust, and mobility during subduction-related melt extraction and later melt metasomatism. While the quantification of V concentrations in xenolith minerals by laser-ablation microprobe inductively-coupled plasma mass spectrometry (LAM-ICPMS) is routine, this destructive analytical technique is not often applied to inclusions in the diamond, where V_2O_5 concentrations determined by electron probe microanalyser (EPMA) are reported instead in some studies.

Cratonic eclogite xenoliths have compositions and element relationships indicating that they originated from various parts of subducted oceanic crust, and eclogitic DI is generally interpreted as derived from cratonic eclogite¹⁶. Geochronological studies utilising radiogenic isotope systematics of DI show that eclogitic diamond formation occurred predominantly in the Mesoarchaean and Palaeoproterozoic^{17,18}. Due to their multi-stage evolution, obtaining reliable dates for eclogite xenoliths is challenging, but nevertheless often successful (for a recent review of ages also for eclogite suites used in this study see ref. 19). Xenoliths and DI show similar ages in various cratons, which in turn correlate with the known timing of Archaean craton amalgamation (Kaapvaal) or Palaeoproterozoic collisional processes at the margins of Archaean cratons (Slave). This has been taken to indicate that diamond formation in eclogite is temporally and genetically linked to the subduction and closure of ocean basins^{7,14,17,20}. In contrast to most DI, the cratonic eclogite reservoir continued to evolve subsequent to diamond formation, mostly through

interaction with fluids and kimberlite-like small-volume melts⁹. This type of metasomatism affected 20–40% of the eclogite reservoir and caused diamond destruction at most xenolith localities²¹, although it can occasionally be associated with abundant diamond growth (e.g., northern Slave craton²²).

Although diamond formation is episodic¹⁶, and younger overgrowths on the eclogitic diamond have been detected by cathodoluminescence and direct dating of diamonds in distinct zones^{23,24}, it is unlikely that the DI used in this study exclusively belong to a late generation of diamond, as also attested by the generally old ages derived from eclogitic inclusions^{7,14}. Thus, it seems plausible that DI record a stage of evolution at least as old as, and likely predating that of, equivalent minerals in eclogite xenoliths, which additionally experienced subsequent mantle metasomatic events.

Here, we exploit published information to assess similarities and differences of V abundances in garnet and clinopyroxene included and protected in diamond, and their xenolithic counterparts, which remained open systems. Underpinned by quantitative modelling, these findings not only have implications for the fO_2 evolution of the subcontinental lithospheric mantle sources of the diamond but also provide intriguing insights into the temperature-, composition- and redox-dependent partitioning behaviour of V in metabasaltic systems, the understanding of which is fundamental to applying V in eclogitic minerals as a redox proxy.

Results

Literature data used to illustrate multi-stage eclogite petrogenesis. Before V in isolated minerals or in bulk rocks can be confidently used as a redox indicator, the underlying controls on V abundances must be understood. To shed more light on this issue, xenoliths and DI are matched for six occurrences in four cratons (Supplementary Data 1). This accounts for the fact that different localities have endemic compositional systematics that reflects the individual origin and evolution of each eclogite reservoir. See Methods for detailed information on the database, an assessment of the two main analytical methods used for the determination of V concentration and the rationale for the reconstruction of bulk eclogite compositions.

Minerals and reconstructed bulk eclogites for xenoliths and corresponding DI show significant differences with respect to multiple variables, summarised in Table 1 and visualised as box-and-whiskers plots in Fig. 1. Various correlations, the suggested causative relationships of which are reviewed below, are summarised in Table 2 and visualised in Supplementary Figs. 1–4. The large scatter and weak resultant correlations reflect the multitude of origins and petrologic processes in eclogite petrogenesis, including, but not limited to (1) an origin as cumulates vs. complementary melts in palaeo-spreading ridges, (2) various degrees of differentiation and melt-rock interactions during the low-pressure stage, (3) various degrees of melt extraction upon subduction in warm Archaean subduction zones. In addition, xenoliths might have been affected by mantle metasomatism. Despite this complexity, we suggest that crystal-chemical, oxygen fugacity and petrologic controls are recognisable in the fact that statistically significant correlations, albeit weak, can still be isolated.

Temperature and crystal-chemical effects on V distribution. A striking observation of the dataset is that median V concentrations in garnet from xenoliths are significantly lower (110 ppm) than those in DI garnet (220 ppm) (Fig. 1b). The average valence and therefore compatibility of V depends on fO_2 , and V becomes more incompatible in common mantle minerals

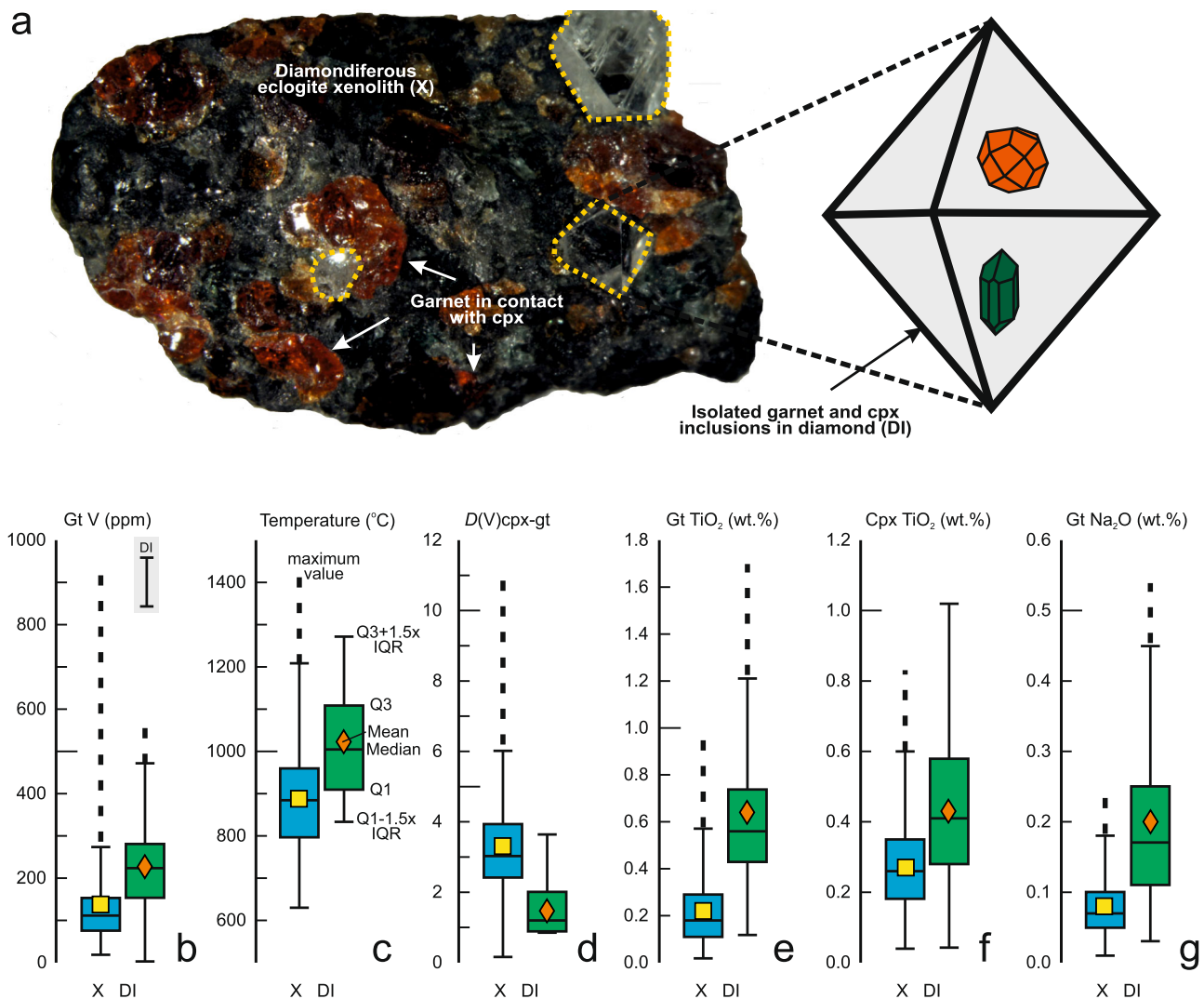


Fig. 1 Illustration of the closed-system behaviour of isolated eclogitic inclusions in diamond (DI) vs. open-system behaviour of touching inclusions in eclogite xenoliths (X). **a** Photograph of a diamondiferous eclogite xenolith from Fort à la Corne (~1.5 cm longest dimension); diamond crystals are highlighted in yellow stipples. Also shown is the schematic of a diamond hosting eclogitic garnet and clinopyroxene inclusions that are non-touching, which prevents them from chemically re-equilibrating to lower temperatures, while the inert diamond also protects them from communicating with the open-system matrix. Contrasting temperature estimates and compositions shown as box-and-whisker plots: **b** Vanadium concentrations (ppm) in garnet (gt), **c** temperature estimates (°C) reflecting those of the eclogite sources at the time of xenolith entrainment in kimberlite, vs. the time of encapsulation of non-touching inclusions in diamond, **d** Distribution (D) of V between clinopyroxene (cpx) and garnet ($D(V)_{\text{cpx-gt}}$), **e** TiO_2 content (wt.%) in garnet, **f** TiO_2 content (wt.%) in clinopyroxene, **g** Na_2O content (wt.%) in garnet. Explanations for the statistical parameters displayed in this figure (mean, median, Q1 first quartile, Q3 third quartile) are shown in panel **c**. The whiskers are here defined as $Q3 + 1.5 \times \text{IQR}$ (interquartile range), and $Q1 - 1.5 \times \text{IQR}$ or the minimum value, whichever is higher; stippled lines extend to the maximum value if $>Q3 + 1.5 \times \text{IQR}$. Average 1σ uncertainty on V abundances in garnet from DI of 117 ppm is shown as error bar; average 1σ uncertainty on V abundances in garnet from xenoliths of 5.6 ppm is not displayed at the scale; both correspond to typical uncertainties for multiple analyses per sample reported in the literature, see Methods). Data sources in Supplementary Data 1.

with increasing $f\text{O}_2$ ¹². As minerals in xenoliths may have interacted with external metasomatic melts, whereas DI are protected inside the inert diamond host, the lower concentration of V in xenolithic garnet relative to DI garnet could, at first glance, be misinterpreted as reflecting a reduction of V abundances due to oxidative metasomatism. However, a notable difference between garnet in eclogitic DI and xenoliths is the higher equilibration temperatures recorded by the former at the time of encapsulation in diamond (median of 1010 °C for DI vs. 890 °C for xenoliths) (Fig. 1c) under generally warmer mantle conditions in Archaean and Palaeoproterozoic time. Indeed, in four of six sample suites, the distribution coefficient D between

clinopyroxene and garnet ($D(V)_{\text{cpx-gt}}$) is significantly negatively correlated with temperature (Supplementary Fig. 1a-b; Table 2), with higher median values for xenoliths (3.0) than for DI (1.2) (Fig. 1d). Despite the considerable scatter, this suggests an underlying temperature control on V incorporation in both clinopyroxene and garnet.

Rutile solubility in garnet from eclogite xenoliths shows a strong positive temperature dependence, such that garnet in high-temperature eclogites has higher TiO_2 contents²⁵, and rutile is known to be an important V host²⁶. Median TiO_2 contents in DI garnet (0.56 wt.%) are higher than those in xenolith garnet (0.18 wt.%) (Fig. 1e), and TiO_2 in garnet is

Table 1 Salient parameters of clinopyroxene, garnet and reconstructed whole rocks in eclogite xenoliths and inclusions in diamond (DI), as well as temperature- fO_2 estimates from the literature (references in Supplementary Data 1).

	Clinopyroxene					Cpx/Gt
	TiO ₂	Al ₂ O ₃ /FeO ^t	Mg#	Jd	V	D(V)
Unit	wt.%				ppm	
Xenoliths <i>n</i> =	261	261	261	261	261	261
Min	0.04	0.4	0.6	0.13	14	0.16
Max	0.83	15.5	0.94	0.58	1050	10.9
Mean	0.27	2.9	0.83	0.31	360	3.4
1σ	0.11	2.8	0.06	0.11	178	1.83
Median	0.26	1.87	0.84	0.31	350	3
DI <i>n</i> =	85	85	85	85	87	17
Min	0.04	0.21	0.65	0.05	68	0.86
Max	0.84	14.7	0.92	0.45	560	2.8
Mean	0.43	1.57	0.78	0.26	320	1.47
1σ	0.2	2.1	0.06	0.11	114	0.63
Median	0.41	1.17	0.78	0.27	320	1.2
Means different? ^a	Yes	Yes	Yes	No	Yes	Yes
	Garnet					V
	TiO ₂	Al ₂ O ₃ /FeO ^t	Na ₂ O	Mg#	Ca#	
Unit	wt.%	wt.%	wt.%			ppm
Xenoliths <i>n</i> =	258	259	255	259	259	261
Min	0.02	0.83	0.01	0.25	0.06	19
Max	0.99	3.4	0.24	0.81	0.51	920
Mean	0.22	1.6	0.08	0.61	0.2	141
1σ	0.14	0.45	0.04	0.1	0.09	123
Median	0.18	1.49	0.07	0.63	0.19	110
DI <i>n</i> =	135	135	135	135	135	134
Min	0.12	0.91	0.03	0.39	0.05	95
Max	1.7	2.7	0.54	0.81	0.58	560
Mean	0.63	1.45	0.2	0.57	0.24	230
1σ	0.30	0.35	0.12	0.09	0.11	99
Median	0.56	1.38	0.17	0.56	0.23	220
Means different? ^a	Yes	Yes	Yes	Yes	Yes	Yes
	Reconstructed whole rocks ^b				Oxythermobarometry ^c	
	Al ₂ O ₃ /FeO ^t	MgO	V	Eu/Eu*	Log fO_2	T
Unit	wt.% basis	wt.%	ppm		ΔFMQ	°C
Xenoliths <i>n</i> =	258	258	260	258	59	259
Min	0.84	5.5	35	0.69	-5.6	630
Max	4.3	18.6	670	2.70	-1.3	1440
Mean	1.74	12.4	250	1.14	-3.3	890
1σ	0.6	2.6	115	0.29	0.96	126
Median	1.57	12.2	230	1.07	-3.3	890
DI <i>n</i> =	18	18	17	5		18
Min	0.87	8.1	95	0.94		830
Max	2.5	16	480	1.15		1270
Mean	1.32	12	270	1.03		1020
1σ	0.38	2.2	105	0.09		136
Median	1.32	11.9	250	0.99		1010
Means different? ^a	Yes	No	No	Yes	Na	Yes

Mg# Mg/(Mg + Fe^{total}), Jd jadeite component in clinopyroxene (cpx), Ca# Ca/(Ca + Mg + Fe^{total} + Mn) in garnet (gt), D distribution coefficient, Eu/Eu* chondrite-normalised Eu/(Sm*Gd)^{0.5} (chondrite of ref. 69).

^aBased on two-tailed t-test for null hypothesis that the means of two populations are equal, and imposing alpha = 0.05 (below which the null hypothesis is rejected), using either equal or unequal variances depending on F-test outcomes

^bBulk rocks are reconstructed with 0.55 garnet, 0.45 clinopyroxene minus half the weight of rutile each (e.g., for 1 wt.% rutile 0.545 garnet, 0.445 clinopyroxene); for V reconstruction, estimated rutile modes and concentrations in rutile were considered.

^cOxygen fugacities as reported or recalculated relative to the Fayalite-Magnetite-Quartz (FMQ) buffer using the eclogite oxybarometer of ref. 70; temperatures are derived using the thermometer of ref. 51 in iterative solution with regional conductive model geotherms (see ref. 21).

Table 2 Pearson correlation coefficients and statistical significance test for various variables discussed in the text (references in Supplementary Data 1).

Suite	$D(V)_{\text{cpx-gt}}-T$ (°C)			Gt TiO ₂ (wt.%)– T (°C)			Gt V (ppm)–Ca# ^a			Gt Na ₂ O (wt.%)– T (°C)		
	<i>r</i>	<i>n</i>	<i>p</i>	<i>r</i>	<i>n</i>	<i>p</i>	<i>r</i>	<i>n</i>	<i>p</i>	<i>r</i>	<i>n</i>	<i>p</i>
1	0.6	36	<0.001	0.22	36	0.196	0.11	34	0.543	0.63	32	<0.001
2	0.22	154	0.006	0.23	154	0.005	0.15	151	0.067	0.32	154	<0.001
3	0.86	27	<0.001	0.5	27	0.007	0.92	21	<0.001	0.83	27	<0.001
4	0.16	20	0.488	0.66	21	0.001	0.46	20	0.041	0.84	21	<0.001
5	0.77	24	<0.001	0.85	15	<0.001	0.38	24	0.067	0.55	24	0.006
6	0.1	15	0.718	0.28	24	0.186	0.19	15	0.488	0.3	15	0.271

	Gt V (ppm)–TiO ₂ (wt.%)			Gt V (ppm)–Na ₂ O (wt.%)			Gt Na ₂ O–TiO ₂ (wt.%)		
	<i>r</i>	<i>n</i>	<i>p</i>	<i>r</i>	<i>n</i>	<i>p</i>	<i>r</i>	<i>n</i>	<i>p</i>
1	0.88	61	<0.001	0.42	57	0.001	0.66	61	<0.001
2	0.53	181	<0.001	0.45	182	<0.001	0.93	181	<0.001
3	0.67	61	<0.001	0.57	61	<0.001	0.86	61	<0.001
4	0.18	26	0.385	0.32	26	0.106	0.76	27	<0.001
5	0.48	41	0.001	0.27	41	0.083	0.74	41	<0.001
6	0.41	22	0.059	0.47	22	0.027	0.8	22	<0.001

	$D(V)_{\text{cpx-gt}}-fO_2$			Cpx V (ppm)– fO_2			Gt V (ppm)– fO_2			WR V (ppm)– fO_2		
	<i>r</i>	<i>n</i>	<i>p</i>	<i>r</i>	<i>n</i>	<i>p</i>	<i>r</i>	<i>n</i>	<i>p</i>	<i>r</i>	<i>n</i>	<i>p</i>
All	0.23	59	0.083	0.34	59	0.008	0.48	59	<0.001	0.41	59	0.001

Suites: 1—Kaaapaal craton kimberlite-hosted, 2—Kaaapaal craton orangeite-hosted, 3—Zimbabwe craton, 4—Northern Slave craton, 5—Central Slave craton, 6—Superior craton.
r—Pearson correlation coefficient, *n*—number of observations, *p*—*p*-value for statistical significance testing, whereby a value of ≤ 0.05 is taken to indicate statistical significance (i.e., the null hypothesis of no significant correlation is rejected).
Cpx clinopyroxene, Gt garnet, Ca# molar Ca/(Ca + Mg + Fe^{total} + Mn), *D* distribution coefficient, oxygen fugacity values fO_2 and temperatures as in Table 1.
^aXenoliths only to minimise superposition of temperature effects.

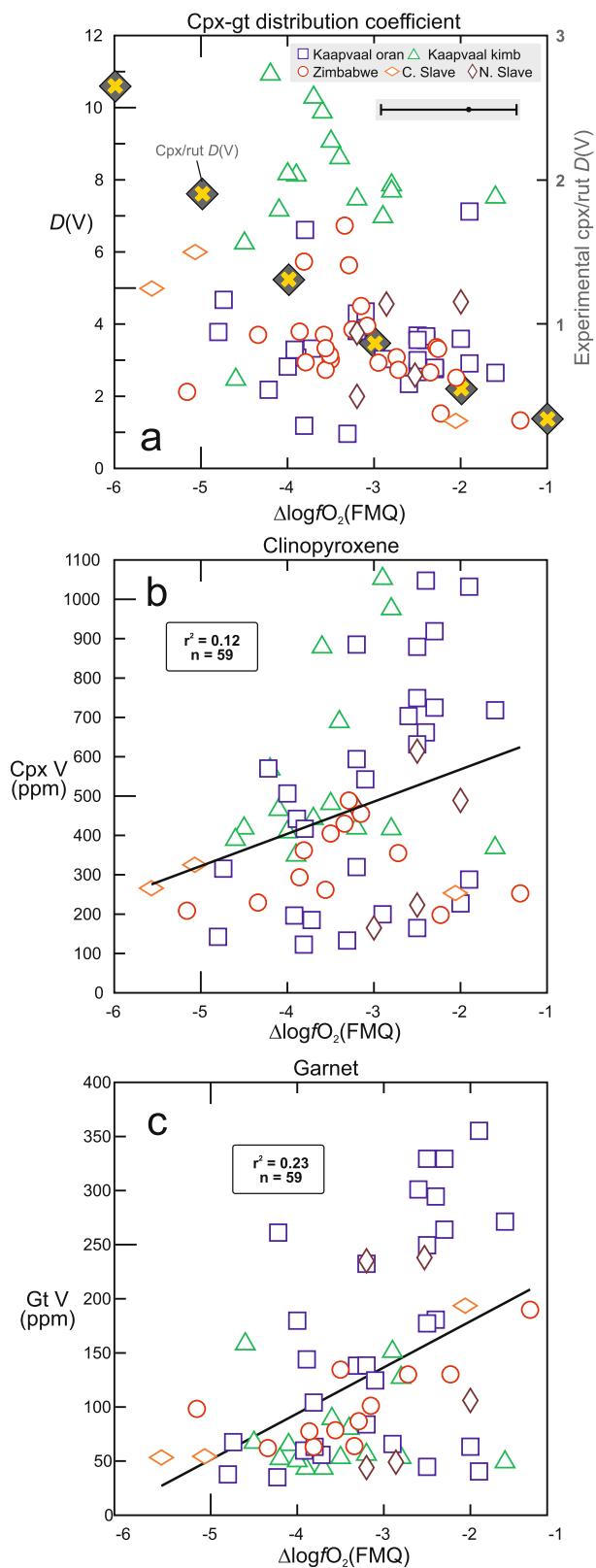
significantly positively correlated with temperature in four of six sample suites (Table 2), similar to V abundances in garnet (Supplementary Fig. 1c–d). In contrast, rutile solubility into clinopyroxene with increasing temperature is weaker²⁵, and the difference between median TiO₂ contents in DI clinopyroxene (0.41 wt.%) and xenolithic clinopyroxene (0.26 wt.%) is correspondingly smaller (Fig. 1f; Table 2). With a median estimated rutile V abundance of 1240 ppm in xenoliths (Supplementary Data 1), the amount of V added to garnet if all rutile (median 0.25 wt.%) were completely dissolved in 55 wt.% garnet (the mode used in bulk rock reconstruction; see Methods) would be ~6 ppm. This alone cannot account for the difference between DI and xenolithic garnet, and therefore crystal-chemical effects in addition to rutile-solubility effects are required.

Higher CaO contents in garnet, here gauged by its molar Ca# (Ca/(Mg + Fe^{total} + Ca + Mn)), facilitate incorporation of incompatible trace elements^{21,25,27}. Consideration of xenoliths only, to minimise superposition of effects from higher average temperatures recorded for DI, reveals a significant negative correlation of garnet V abundance with Ca# for two of six sample suites (Table 2), which translates into a negative correlation of $D(V)_{\text{cpx-gt}}$ with garnet Ca# (Supplementary Fig. 1e–f). Finally, Na₂O uptake in garnet is temperature-dependent²⁵, as borne out by significant differences in Na₂O content for garnet in xenoliths and DI (Fig. 1g), and by positive correlations between Na₂O content and temperature for five of six sample suites (Supplementary Fig. 1g–h; Table 2). High V abundances in garnet are correlated to high TiO₂ and Na₂O contents (significant for four of six suites each), whereby groups of samples deviate from this pattern (Supplementary Fig. 1i–l; Table 2). The temperature effect may be indirect, via increased uptake of TiO₂ and Na₂O contents in garnet, which might enhance V abundances as part of various coupled substitutions.

Oxygen fugacity effects on V partitioning in eclogitic minerals.

In contrast to homovalent trace elements, $D(V)_{\text{cpx-gt}}$ may also depend on fO_2 , as it does for mineral-melt pairs because fO_2 determines the average valence state and cation size, which in turn determines the fit into various lattice sites available in minerals^{28–31}. For further insights into fO_2 effects on $D(V)$, we consider both experimental and natural mineral pairs. The combination of parameterisations of experimental clinopyroxene-melt and rutile-melt $D(V)$ ^{12,26} as a function of fO_2 (both obtained at 1300 °C) reveals a marked increase in clinopyroxene/rutile $D(V)$ with decreasing fO_2 , relative to the Fayalite-Magnetite-Quartz buffer expressed as $\Delta \log fO_2$ (FMQ), from 0.20 at FMQ-1 to 1.9 at FMQ-5. This roughly corresponds to the fO_2 range in eclogite xenoliths in this study (Fig. 2a; Supplementary Data 1). In contrast, $D(V)_{\text{cpx-gt}}$ in eclogite xenoliths shows no significant correlation with fO_2 when all data are considered (Table 2), but a weak one ($r^2 = 0.26$, $n = 15$) for samples from the Zimbabwe and the central Slave cratons. While V abundances in clinopyroxene show a very weak dependence on fO_2 ($r^2 = 0.12$; $n = 59$; Fig. 2b; Table 2), those in garnet show a stronger positive correlation ($r^2 = 0.23$; $n = 59$; Fig. 2c; Table 2). The scatter likely reflects superposed crystal-chemical controls unrelated to fO_2 effects, as discussed above, and various petrologic processes affecting the cratonic eclogite reservoir from its beginnings at mid-ocean ridges to exhumation with the host magma (next sections).

Despite the scatter, the fO_2 –V relationships in Fig. 2 suggest that an increase in fO_2 facilitates V uptake in garnet and rutile, more so than in clinopyroxene. The observed decrease in experimental $D(V)_{\text{cpx-rutile}}$ may indicate a decreasing misfit with respect to the octahedral site occupied by Ti in rutile³². It is uncertain whether the fO_2 increase is accompanied by an increase in the average V valence state in garnet. Exclusively trivalent V in octahedral coordination is found in Fe³⁺-rich



garnet of the schorlomite species representing garnet at fairly oxidised conditions³³. Richter et al.²⁹ investigated the partitioning of V between garnet and silicate melt at high pressure and found a marked decrease in V compatibility in garnet with increasing fO_2 . Nevertheless, garnet in the experiments and in natural peridotite was found to have a rather constant average V valence

Fig. 2 Effects of oxygen fugacity on the distribution and abundances of V in eclogite minerals. **a** Distribution D of V between clinopyroxene (cpx) and garnet (gt) in eclogite xenoliths as a function of oxygen fugacity relative to the Fayalite-Magnetite-Quartz buffer ($\Delta\log fO_2$ (FMQ); available for xenoliths only); oran-orangeite-hosted, kimb-kimberlite-hosted. Superposed is the distribution of V between clinopyroxene and rutile (rut) as a function of fO_2 (yellow crosses), as calculated from the parameterisation of experimentally determined mineral-melt partition coefficients^{12,26}. Vanadium concentration (ppm) in **b** clinopyroxene and **c** garnet as a function of fO_2 , with regressions and r^2 (significant for the number n of observations; Table 2). Error bar in **a** shows representative average 1σ uncertainty of fO_2 estimates of $-1.0, +0.6$ ¹⁴; 1σ uncertainties on V abundances of 14.5 ppm for clinopyroxene and 5.6 ppm for garnet (corresponding to typical uncertainties for multiple analyses per sample reported in the literature, see Methods) are small relative to the depicted scale and not shown. Data sources in Supplementary Data 1.

state of $\sim+2.5$ (i.e., $\sim 50\% V^{2+}$ and $50\% V^{3+}$) over an extended fO_2 range between FMQ-4.5 to FMQ-1.8, suggesting that crystal-chemistry exerts a stronger control on V valence in garnet than fO_2 ²⁹.

Identifying cumulate vs. melt protoliths. As mentioned above, eclogite xenoliths are interpreted as metamorphic products of subducted oceanic crust composed of extrusive and intrusive sections⁶, and the same applies to Archaean eclogitic diamond substrates¹⁰. Prior eclogite xenolith work gauged the importance of plagioclase accumulation based on Eu/Eu^* (chondrite-normalised $Eu/(Sm^*Gd)^{0.5}$), which exploits the greater compatibility of Eu than neighbouring REE in plagioclase, and on low abundances of HREE, which are incompatible during accumulation. However, only a few studies report trace-element data for DI. As plagioclase-rich rocks with low HREE abundances, such as MOR gabbros, also have high Al_2O_3/FeO (Supplementary Fig. 2), this ratio can serve as an alternative proxy to detect cumulate processes during protolith formation. A plot of V vs. Al_2O_3/FeO in reconstructed whole rocks illustrates low V abundances in samples with gabbroic protoliths, and also highlights a higher proportion of such protoliths for xenoliths than for DI (Fig. 3a–b; Table 1). The trend of low V-high Al_2O_3/FeO in eclogites with cumulate protoliths to high V-low Al_2O_3/FeO in eclogites with melt protoliths mimics that of natural MOR gabbros and MORB, save some reconstructed bulk eclogites from the Kaapvaal and northern Slave cratons showing anomalous V enrichment (Fig. 3a–b). These systematics are also recognisable in clinopyroxene and garnet alone (Supplementary Fig. 2). Thus, lower V in xenolithic garnet than in DI garnet is the result not only of temperature and crystal-chemical effects, as discussed above, but also of greater importance of cumulate processes during protolith formation.

The higher proportion of gabbroic protoliths in eclogite xenoliths than in eclogitic DI is statistically significant (Table 2) and therefore unrelated to sampling issues. Furthermore, a gabbroic signature is also evident for a higher proportion of diamondiferous eclogites than DI³⁴. This suggests that it is not the diamond-forming process itself that modifies the eclogite substrate. Instead, in a model of eclogitic diamond formation via flushing of oceanic crust with dehydration fluids derived from the underlying serpentinised oceanic mantle²¹, it might reflect that fluids are initially solute-poor as they enter the gabbroic lower oceanic crust, leading to the formation of inclusion-free diamond. One may speculate that such fluids reach carbon saturation in all parts of the oceanic crust but become more solute-rich by the

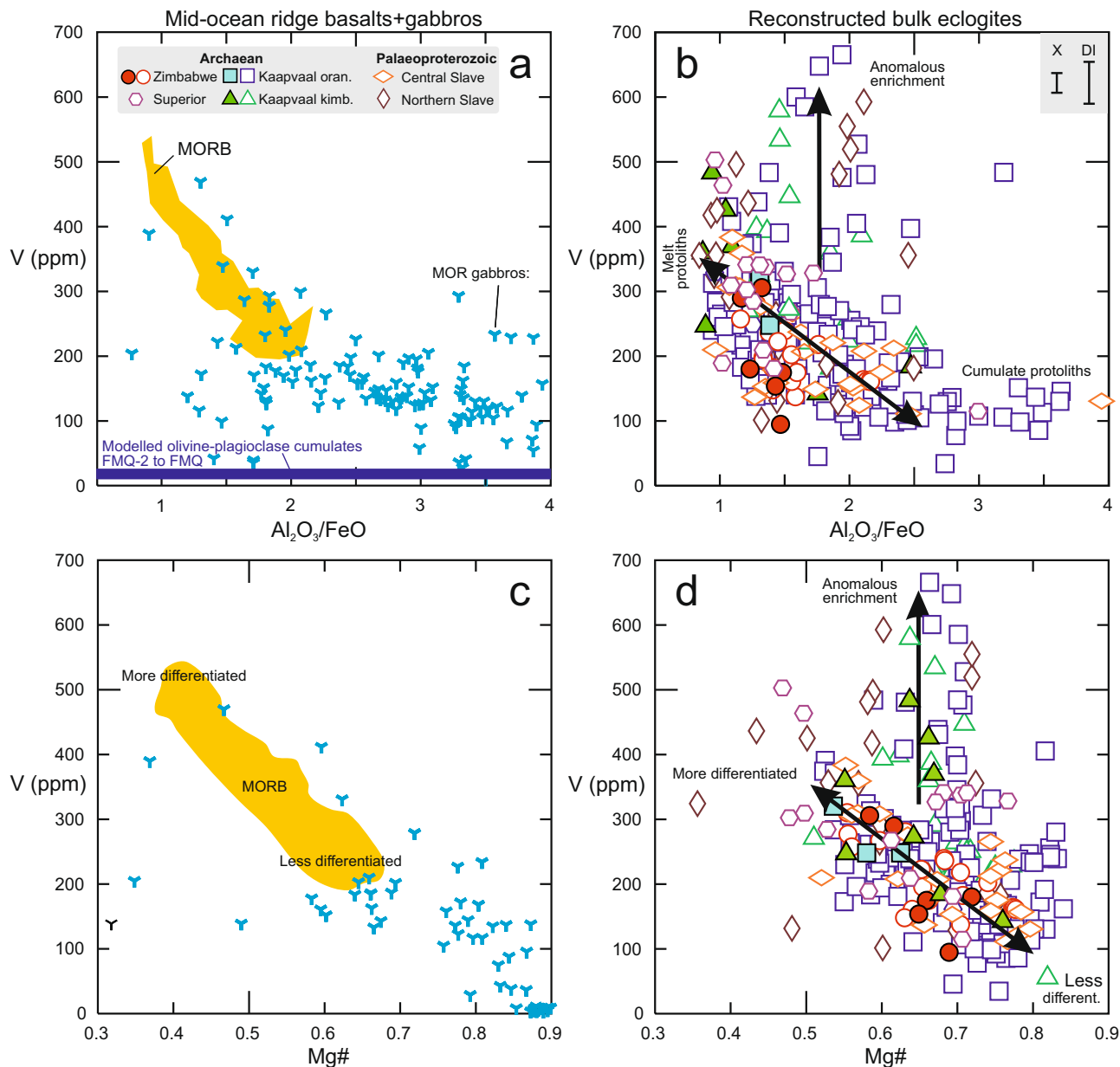
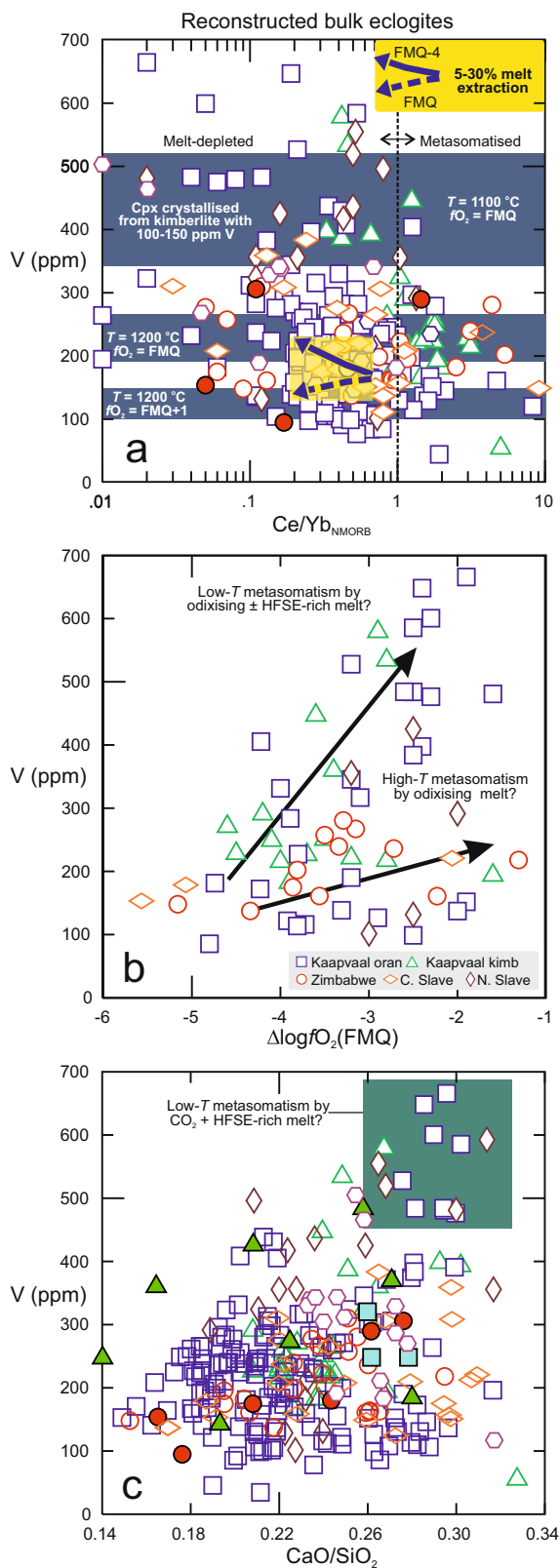


Fig. 3 Effects of low-pressure accumulation and differentiation on V abundances in eclogite protoliths. Vanadium abundances (ppm) in **a** mid-ocean ridge basalts (MORB; yellow field⁷¹) and MOR gabbros (blue tristrars, $Eu/Eu^* > 1.05$; from PetDB: www.earthchem.org/petdb), and **b** reconstructed bulk compositions of eclogite xenoliths (X) and inclusions in diamond (DI) as a function of Al_2O_3/FeO . Eclogites with suggested gabbroic cumulate vs. melt protoliths, and those showing inferred anomalous enrichment, are indicated in **b**. Shown in **a** is the range of compositions for olivine+plagioclase accumulating from a parental melt formed at $\Delta \log fO_2(FMQ) -2$ to 0 (dark blue bar at bottom; modelling parameters and rationale in Methods; Supplementary Table 2). Vanadium abundances (ppm) in **c** MORB (yellow field) and MOR gabbros (blue tristrars), and **d** reconstructed bulk eclogite xenoliths and DI as a function of molar $Mg\#$ ($Mg/(Mg + Fe^{total})$), a proxy for the degree of differentiation during protolith formation. Eclogites with suggested less and more differentiated protoliths, and those showing inferred anomalous enrichment, are indicated in **d**. Error bars for reconstructed bulk rocks in **b** show average propagated 1σ uncertainties on V abundances of 29 ppm for xenoliths and 69 ppm for DI (Methods). Data sources in Supplementary Data 1.

time they infiltrate the upper oceanic crust, enabling the precipitation of inclusion-bearing diamonds.

Effects of petrologic processes on V abundances in eclogite. In order to assess petrologic effects on V abundances, we model the behaviour of V during the formation and differentiation of oceanic crustal protoliths, as well as during subsequent melting in subduction zones, and metasomatism during their residence in the lithospheric mantle. Mineral-melt $D(V)$ during partial

melting of the mantle depends not only on fO_2 but also on temperature³⁵. Both parameters have changed through geologic time^{14,15,36,37}, with a suggested lower end of shallow upper mantle fO_2 of $\sim FMQ-2$ and mantle potential temperature of $T_p \sim 1450^\circ C$ at the time of dominantly Mesoarchaean emplacement of oceanic crust now sampled as eclogite xenoliths. Entering these parameters into the spreadsheet of ref. ³⁵, which uses a Depleted Mantle starting composition with 73 ppm V and calculates mineral-melt $D(V)$ as a function of temperature and fO_2 , the parental melt is modelled to have ~ 170 ppm V for a melt fraction



of 0.2 (see Supplementary Table 1 and Methods for modelling parameters and rationale). For comparison, the parental melt of modern MORB at $F = 0.08$, $T_p = 1300\text{ }^{\circ}\text{C}$ and $fO_2 = \text{FMQ}$ would have ~ 200 ppm V. This relatively small difference reflects competing effects of stronger V compatibility in the solid at lower T_p but stronger V incompatibility at higher fO_2 during mantle

Fig. 4 Effects of partial melt extraction and metasomatism on V abundances in eclogites. **a** Vanadium abundances (ppm) in reconstructed bulk eclogite xenoliths and DI as a function of normal mid-ocean ridge basalt (NMORB)-normalised Ce/Yb, a proxy for melt depletion and enrichment. Shown for comparison is the modelled trend (yellow box) for partial melt extraction from rutile-eclogite, with a moderate decrease of V abundances at relatively oxidising conditions of $\Delta\log fO_2(\text{FMQ}) = 0$, similar to the modern ambient mantle⁷². For $\Delta\log fO_2(\text{FMQ}) = -4$, at the low end of fO_2 estimates for eclogite xenoliths, partial melt extraction from eclogite causes an increase in V abundances (modelling parameters and rationale in Methods; Supplementary Table 4). Also shown is the effect of metasomatism, as mediated by crystallisation of a high-temperature pyroxene from a kimberlite melt²¹ with 100–150 ppm V⁶⁶; V abundances in the metasomatic clinopyroxene are calculated for various temperature and fO_2 conditions, shown with grey-blue fields (modelling parameters and rationale in Methods; Supplementary Table 5); reconstructed pre-metasomatic eclogites ($\text{Cr}_2\text{O}_3 < 0.1$ and $\text{Ce}/\text{Yb}_{\text{NMORB}} < 1$) would have 280 ± 140 ppm V. NMORB for normalisation from ref. ⁶⁰. **b** V abundances (ppm) in reconstructed bulk eclogite xenoliths as a function of oxygen fugacity relative to the Fayalite-Magnetite-Quartz buffer ($\Delta\log fO_2(\text{FMQ})$; no combined fO_2 -V information available for DI), showing an overall positive correlation (significant, see Table 2). Arrows qualitatively indicate effects of melt metasomatism via clinopyroxene addition under various conditions as shown in **a** (HFSE-high field-strength elements). **c** V abundances (ppm) in reconstructed bulk eclogite xenoliths and DI as a function of CaO/SiO₂, a proxy for metasomatism by CO₂-rich melt⁴⁹; note samples with anomalous V enrichment are restricted to high ratios (teal-coloured field). Average propagated 1σ uncertainties on V abundances are 29 ppm for xenoliths and 69 ppm for DI (Methods). Data sources in Supplementary Data 1.

melting for modern compared to Archaean oceanic crust formation.

The crystallisation sequence at pressures < 0.5 GPa in dry peridotite-derived melts, typical for spreading ridges, is spinel, olivine, plagioclase and clinopyroxene. So long as only spinel, olivine and plagioclase are on the liquidus (over some 50% of crystallisation), the solid-melt bulk partition coefficient for V is very low (< 0.15) for reasonable Archaean conditions ($fO_2 = \text{FMQ}-2$ to FMQ ; $T_p = 1450\text{--}1400\text{ }^{\circ}\text{C}$), resulting in a modelled cumulate rock with < 30 ppm V (Methods; Supplementary Table 2; Fig. 3a). This is lower than the ~ 100 ppm for reconstructed eclogite xenoliths with high $\text{Al}_2\text{O}_3/\text{FeO}$ and therefore plagioclase-rich cumulate protoliths (Fig. 3b). Although higher T_p results in higher V in the melt, this is to some extent offset by lower mineral-melt $D(V)$ during crystallisation at correspondingly higher temperatures. The gabbroic protoliths may therefore have experienced the addition of trapped melt and/or reactive crystallisation of clinopyroxene ($\sim 110\text{--}580$ ppm V at the modelled conditions), as postulated for modern MOR gabbros³⁸. Still, MOR cumulates have low V, which is then inherited by eclogite upon metamorphism.

Due to the low olivine- and plagioclase- $D(V)$, the fractionation of these minerals during oceanic crust formation leads to an increase in melt V abundances (Methods; Supplementary Table 3). Differentiation along with olivine \pm plagioclase control lines during protolith formation may explain why Mg# in garnet, clinopyroxene and whole rocks is anti-correlated with V abundances (Fig. 3c–d, Supplementary Fig. 3). For reconstructed whole rocks, this trend again mimics that observed in modern MORB and MOR gabbros, again with deviations for some samples from the Kaapvaal and northern Slave cratons. The considerable scatter in the natural samples probably reflects the superposition of additional processes, such as partial melt

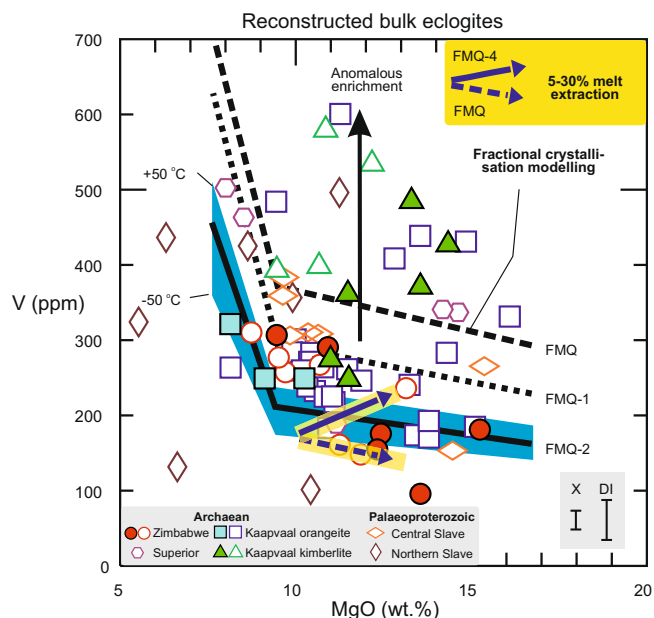


Fig. 5 Estimates of fO_2 of convecting mantle sources from which the oceanic crustal protoliths to eclogites formed. Shown are V abundances (ppm) in reconstructed bulk eclogite xenoliths and DI as a function of MgO content (wt.%), filtered to exclude samples with gabbroic cumulate protoliths (conservative cut-off $Al_2O_3/FeO = 1.7$) and, for xenoliths, metasomatism (NMORB-normalised $Ce/Yb > 1$ and $Cr_2O_3 > 0.1$ wt.%). Shown for comparison is the modelled evolution of melts for a mantle potential temperature (T_p) of 1450 °C (olivine crystallisation temperature of 1340 °C) after crystallisation of spinel, olivine and plagioclase from a parental melt formed at a melt fraction of 0.2, appropriate for warmer Archaean spreading ridges, and various fO_2 . A difference of ± 50 °C in T_p and corresponding crystallisation temperature is shown as blue envelope for $\Delta \log fO_2(FMQ) = -2$, whereby V becomes more incompatible with increasing temperature³⁵, causing the isopleths to shift upward relative to samples. Modelled effect of 30% melt extraction at FMQ-4 and FMQ (as in Fig. 4a) is shown for comparison (purple arrows), illustrating that melt extraction at FMQ-4 biases V abundances toward higher apparent fO_2 whereas at FMQ melt extraction shifts samples with MgO $> \sim 9$ wt.% along olivine control lines. Modelling parameters and rationale in Methods; Supplementary Table 3. Error bars for reconstructed bulk rocks show average propagated 1σ uncertainties on V abundances of 29 ppm for xenoliths and 69 ppm for DI (Methods). Data sources in Supplementary Data 1.

extraction during subduction of oceanic crust, and metasomatism after its capture in the lithospheric mantle.

Melt extraction during subduction decreases the LREE/HREE ratio because of the incompatibility of LREE and the compatibility of HREE in a rock consisting of subequal volumes of clinopyroxene and garnet (Fig. 4a). Modelling shows that this process leads to moderately decreasing V abundances in the residue (e.g., from 170 ppm in the protolith to 140 ppm after 30% of melt extraction), at relatively oxidising conditions of $fO_2 = FMQ$, and to insignificant changes (to 176 ppm) for FMQ-1, but increasing V abundances for lower fO_2 (to 230 ppm for FMQ-4) (Fig. 4a; Methods; Supplementary Table 4). The modelled changes due to partial melt extraction are small relative to the range displayed by natural samples and therefore do not appear to be the dominant control on V abundances in eclogite xenoliths or DI.

It has been inferred that the compositional relationships in metasomatised eclogite xenoliths are best satisfied if magmatic

clinopyroxene is added from a kimberlite-like melt²¹. The parameterisation of ref. 35 demonstrates that V concentrations in clinopyroxene in equilibrium with melt would vary strongly not only as a function of fO_2 but also of temperature. Modelling shows that the addition of such clinopyroxene would most strongly increase V abundances in eclogite for reducing and cool conditions when V behaves most compatibly (Fig. 4a; Methods; Supplementary Table 5).

Discussion

Earlier work suggested generally more reducing conditions in the Archaean convecting mantle than today. This is based on low V/Sc and $Fe^{3+}/\Sigma Fe$ in unmetasomatised, non-cumulate and little-differentiated (meaning only olivine \pm plagioclase fractionation) eclogite specimens¹⁴, and on fO_2 estimates from komatiites, picrites and basalts of various ages^{15,39}. When the effects of accumulation and fractional crystallisation during protolith formation are accounted for, by considering V abundances as a function of Al_2O_3/FeO and Mg#, respectively, there are no systematic differences between xenoliths and DI (Fig. 3). Instead, eclogite compositions reconstructed from both xenoliths and DI predominantly follow trends recognised also in modern MORB and MOR gabbro, although a subset shows anomalous enrichment that is discussed below. In Fig. 5, all reconstructed bulk eclogites were filtered for accumulation, and xenoliths additionally for metasomatism, for a meaningful comparison to forward models of differentiating mantle-derived melts. Most of the Archaean data fall between modelled fO_2 isopleths of $\sim FMQ-1$ to $FMQ-2$ (Fig. 5). In contrast, Palaeoproterozoic eclogites from the central Slave craton mostly fall between $\sim FMQ-1$ to FMQ , while those from the northern Slave craton show significant scatter (see next section).

Melt loss from eclogite at FMQ would cause a decrease in V abundance that parallels that of olivine control lines, causing little change in apparent source fO_2 (Fig. 5). Conversely, melt loss from eclogite at $fO_2 \leq FMQ-1$, corresponding to those determined for the vast majority of samples, would increase V abundances, biasing the results towards a higher apparent source fO_2 . This suggests that in carefully filtered databases lacking information on geochemically similar homovalent elements (e.g., Sc), V alone can be used to illustrate redox-related igneous processes and capture the maximum fO_2 signature of the convecting mantle source from which the igneous protoliths were derived.

In cratonic eclogite, mantle metasomatism, typically by kimberlite-like melts, often causes Cr_2O_3 and LREE enrichment (e.g., NMORB-normalised $Ce/Yb > 1$), and is thought to be mediated by the precipitation of a high-temperature pyroxene²¹. Mantle metasomatism is often associated with oxidation^{40,41}, although both oxidising and reducing metasomatism occurs, based on garnet oxybarometry applied to peridotite xenoliths⁴². For oxidising metasomatism by carbonated melts, a corresponding decrease of V abundances in olivine and two pyroxenes from garnet-free peridotite xenoliths has been documented⁴³. This is consistent with experiments, where peridotite minerals show a strong decrease in mineral-melt $D(V)$ with increasing fO_2 across the fO_2 range relevant to the cratonic mantle¹². In contrast, this study makes the intriguing observation that with increasing fO_2 , V abundances in eclogite minerals (Fig. 2b, c) and bulk rocks (Fig. 4b) from some suites show a mild but statistically significant increase (Table 2) or remain constant for others.

The seemingly paradoxical effect of increasing V abundances with fO_2 in some xenolithic eclogite suites may result from the stability of low-volume, carbonated oxidising melts in eclogite to temperatures that are lower by several 100 °C than temperatures required for stabilisation of higher-volume, carbonate-poor and

therefore less oxidising melts⁴⁴. Vanadium concentrations in pyroxene precipitated from a kimberlite melt with 100–150 ppm V under cool conditions (1100 °C) would be V-rich even at relatively high fO_2 of FMQ (e.g., 350–530 ppm), but much lower for higher melt-rock reaction temperatures of 1200 °C (180–280 ppm; Fig. 4a). For comparison, reconstructed pre-metasomatic eclogites, i.e., those having $Cr_2O_3 < 0.1$ and $Ce/Yb_{NMORB} < 1$, have V concentrations of 280 ± 140 ppm. Metasomatic clinopyroxene can therefore increase or dilute V abundances in eclogite, depending not only on fO_2 but also on the temperature conditions under which it was added. This may explain why oxidative metasomatism in mantle eclogite causes no consistent change in the V abundance of the affected eclogite, and can even cause an increase in V abundances in some samples (Fig. 4b), in contrast to the decrease observed in peridotite with generally higher solidus temperatures⁴⁵.

It is conspicuous that eclogite xenoliths from the northern Slave craton and some samples from the Kaapvaal craton show anomalous enrichment in V, extending to concentrations beyond those in any DI garnet (Fig. 3). Eclogite xenoliths from the Slave craton have been previously noted for their unusual HFSE enrichment during interaction with CO_2 -rich melt soon after subduction and metamorphism⁴⁶, and it seems that V was enriched along with Nb and Zr. In the Kaapvaal craton, anomalous V enrichment may be linked to the formation of MARID rocks (Mica-Amphibole-Rutile-Ilmenite-Diopside) around the time of orangeite magmatism^{47,48}. In both cratons, the enrichment would be related to an external, HFSE-enriched melt, which does not appear to impart elevated Ce/Yb (Fig. 4a). Nevertheless, the involvement of a silica-undersaturated, CO_2 -rich agent is supported by the observation that eclogites with the highest V abundances are restricted to elevated CaO/SiO₂, a hallmark of carbonatite metasomatism⁴⁹ (Fig. 4c).

Diamond formation is a metasomatic process involving COH fluids or melts^{3,10}. However, once formed, a diamond is a robust container for inclusions. In contrast, the mantle as sampled by xenoliths at the time of kimberlite entrainment has remained an open system. In this light, it is somewhat surprising that most reconstructed bulk xenoliths and DI show similar V abundances at similar Al_2O_3/FeO and Mg#, i.e., after accounting for effects of low-pressure accumulation and differentiation (Fig. 3). This retention of low-pressure signatures in both xenoliths and DI attests to the robustness of V during processes after the ocean floor stage. The overall similarity of V abundances in xenoliths and DI may thus point to an oxygen-conserving mechanism for eclogitic diamond formation, for example via mixing, or cooling of CO_2 - and CH_4 -bearing fluids near the water maximum^{2,3}. The implication is that diamond formation does not appear to alter the fO_2 of the eclogites.

The similarity of V abundances in DI and xenoliths further suggests that V concentrations in the cratonic eclogite reservoir globally—and fO_2 conditions—did not change systematically subsequent to the diamond formation, despite the scatter in V abundances and fO_2 imposed by metasomatism. The implication is that the mantle eclogite reservoir, and by inference subducted oceanic crust, is a system that is efficiently buffered to O_2 introduced over aeons of subduction- and mantle-related metasomatic processes. Instead, these processes lead to the formation of diamonds at the low fO_2 recorded by eclogite xenoliths. This is what makes eclogite a supreme diamond source rock, in addition to being a faithful recorder of the origin, evolution and fate of ancient subducted ocean basins.

Methods

Database. The database for V concentrations in clinopyroxene and garnet inclusions in diamond (DI) is comprised of 87 clinopyroxenes (18 with REE data) and

135 garnets (29 with REE data, 2 without reported major element data). These diamonds are mostly sampled as kimberlite-borne xenocrysts in diamond processing facilities, rarely from diamondiferous xenoliths (e.g., refs. 9,50). Of these inclusions, 18 are paired (i.e., separate inclusions in the same diamond that, occasionally, are touching), thus conducive to bulk rock reconstruction and temperature calculation (Supplementary Data 1). Temperatures for clinopyroxene-garnet pairs were obtained using the thermometer of ref. 51, solved iteratively with regional conductive model geotherms (see ref. 21 for rationale and limitations). Here, reported compositions for multiple non-touching inclusions per mineral and diamond were averaged. All of these represent measurements from distinct samples, i.e., reported compositions for multiple inclusions in the same diamond were averaged.

For eclogite xenoliths, the choice of datasets reflects localities for which DI V data are also available, encompassing the Zimbabwe craton, the Kaapvaal craton at the time of Jurassic orangeite and Cretaceous kimberlite magmatism, the Superior craton, and central and northern Slave craton (Supplementary Data 1). Only xenolith datasets with major and trace-element analyses for both clinopyroxene and garnet are considered. Samples showing evidence for kimberlite contamination were filtered (here: Ba or Nb in garnet >0.5 ppm, or Ba or Nb in cpx >1.5 and 1 ppm, respectively)²¹. All data points represent measurements from distinct samples.

Assessment of analytical methods and uncertainty estimates. Vanadium is a multi-valent element, the partitioning of which into minerals vs. melt depends also on its redox state^{11,12}. The following assessment of analytical techniques is centred on V, as abundances derived from mixed techniques are used in this study; these are indicated in Supplementary Data 1.

Published V_2O_3 concentrations in DI were predominantly determined by EPMA. Limits of detection (LOD) for V are not always given; ref. 52 quote 100 ppm, and ref. 53 quote ≤ 136 ppm for all measured oxides. We here apply a blanket LOD of 136 ppm assuming that some lower reported values may actually be $<LOD$. To avoid biasing the DI database toward higher values, we count values <136 ppm as $LOD * \sqrt{2}/2$ (ref. 54), corresponding to 96 ppm. ref. 52 reports external average 1σ uncertainties for EPMA-derived V concentrations (multiple spots per mineral and sample) of 21% and 52% for clinopyroxene and garnet, respectively, which we assign as a blanket uncertainty to EPMA-derived mineral data for all DI (67 ppm for clinopyroxene, 117 ppm for garnet, for their respective mean compositions in the database). The overlap of the TiK β on the VK α peak during wavelength-dispersive spectroscopy implies that V concentrations have to be corrected, for example by analysing a Ti-rich and nominally V-free standard as an unknown to apply a linear correction based on apparent V concentrations (e.g., data reported in ref. 55). Other work (e.g., in ref. 53) employed the software of ref. 56 with the JEOL 8900 R, which makes an automated correction. All EPMA-derived V concentrations have been corrected for Ti overlap either offline or using the software, as indicated in Supplementary Data 1. Reference 35 considers the correction procedure for TiO₂ contents <1.76 wt.% unproblematic. In this study, reported TiO₂ abundances in eclogitic clinopyroxene and garnet DI are relatively low (median 0.43 and 0.64 wt.%, respectively) requiring only moderate correction.

Vanadium is a relatively abundant element in clinopyroxene (average 350 ppm in this study) and garnet (140 ppm) from eclogite xenoliths ($n = 261$), far above typical LOD afforded by laser-ablation microprobe inductively-coupled plasma mass spectrometry (LAM-ICPMS; e.g., average LOD 0.05 ppm for >100 analyses reported in ref. 21). Reference materials were measured as unknowns to monitor accuracy in all xenolith studies included in Supplementary Data 1, and no issues are reported (two DI studies with LAM-derived V abundances do not comment on accuracy). Where available, measured and accepted values for reference materials are given in Supplementary Data 1. Furthermore, the typically high degree of inter- and intra-grain homogeneity affords analysis at high precision (e.g., 4% instrumental, 4% for analysis of multiple spots per grain and multiple grains per sample²¹). For LAM-ICPMS-derived V concentrations we assume a blanket external uncertainty of 4% 1σ (14.5 ppm for clinopyroxene, 5.6 ppm for garnet, for their respective mean compositions in the database).

In order to test the correspondence of LAM- and, after correction, EPMA-derived V abundances, we carried out V_2O_3 analyses at Goethe-University Frankfurt employing the Jeol JXA-8530F Plus Hyperprobe, for which V abundances had been determined by LAM-ICPMS. For this, we chose three mounts from Orapa, which are also used in this study (OE16, OE23, OE34; Supplementary Data 1). The results are reported in Supplementary Table 6. A nominally V-free synthetic rutile standard was used to determine the apparent V abundances resulting from the overlap of TiK β on VK α , using PETL and LIFL crystals, respectively, with average detection limits of 200 ppm (40 s on peak–20 s on background) and 160 ppm (90–45 s), respectively. Apparent V abundances in the synthetic rutile amounted to 2660 ± 68 ppm ($n = 13$), i.e., 26.7 ± 0.7 ppm per wt.% TiO₂, which corresponds to 4% of the total V determined in clinopyroxene, and to 11% in garnet. Compared to LAM-derived V abundances, corrected EPMA-derived abundances determined for clinopyroxene in three samples are higher or lower by $\leq 5\%$ (i.e., without a consistent sign). Corrected EPMA-derived V abundances for garnet in two samples (garnet was not mounted in the third sample) are near and below the detection limit, respectively, with large resultant

uncertainties (190 ± 50 and 110 ± 90 ppm, respectively). They are higher by 3 and 12%, respectively, than LAM-ICPMS-derived concentrations but agree with the uncertainties.

Bulk rock reconstruction and effect of rutile. Conventionally, bulk rocks for xenoliths are reconstructed from mineral modes to avoid the effects of kimberlite contamination⁶, whereas for DI this is required by the nature of the sample. For both types of samples, the same approach is used, assuming 55 wt% garnet and 45 wt% clinopyroxene, as rationalised in ref. ⁵⁷. In the database, the average increase in V related to an estimated 10% uncertainty in the modal proportions of clinopyroxene at the expense of garnet is 21 ppm, or 9%. Consistent with rutile-melt distribution coefficients ($D > 1$) (ref. ²⁶), bulk rocks reconstructed without rutile have minimum V contents. The modal fraction of accessory rutile in a bulk rock having no primary Ti anomaly, as applies to crystallisation from dry peridotite-derived melt in spreading ridges, can be estimated by assuming that Ti is not depleted relative to REE with similar bulk distribution coefficients during partial melting (Sm and Gd)⁵⁷. As the vast majority of clinopyroxene and garnet in the DI database are unpaired, bulk rocks can be reconstructed only for a small subset of samples, and the theoretical amount of rutile in the source cannot be calculated except for the few samples with reported REE concentrations.

The abundances of V in rutile can be estimated from the abundances measured in clinopyroxene and using a distribution coefficient $D(V)$ between clinopyroxene and rutile, assuming these two minerals were in equilibrium. Based on natural clinopyroxene-rutile pairs in 22 eclogite xenoliths, $D(V)$ is 0.283 ± 0.091 ²⁵, which is biased towards available data from the West African and central Slave craton. For samples with independent fO_2 estimates ($n = 59$ in this study), experimental cpx/rutile distribution coefficients can alternatively be used to estimate V abundances in rutile, taking into account the fO_2 -dependent partitioning of V in both minerals^{12,26} (Supplementary Data 1). Bulk rocks ($n = 50$) reconstructed with rutile with a fixed clinopyroxene-rutile $D(V)$ and, alternatively, with fO_2 -dependent D have average V concentrations of 309 and 303 ppm, respectively, which can be considered identical within uncertainties. Since only a subset of samples has fO_2 estimates, we proceed with rutile V estimates from the average clinopyroxene-rutile $D(V)$ determined for eclogite xenoliths.

Uncertainties on V abundances are estimated by propagating the average 1 σ uncertainties on V abundances in garnet and clinopyroxene (52% and 21%, respectively, for DI, 4% for both minerals in xenoliths, see above), weighted by their respective contributions (not considering rutile), and considering a total 10% uncertainty in modal abundances. Clinopyroxene contributes 68% to the bulk in xenoliths, but only 54% to the bulk in DI owing to stronger V partitioning into garnet at higher average temperatures recorded by DI, as discussed in Section Temperature and crystal-chemical effects on V distribution. This results in average 1 σ uncertainties of 29 ppm for reconstructed bulk xenoliths and 69 ppm for DI.

Statistics. Two-tailed t -tests were applied to test the null hypothesis that the means of the two populations (xenoliths and DI, reported in Table 1 along with number n of observations) are equal, using either equal or unequal variances depending on F-test outcomes, where an alpha value of 0.05 was imposed. The significance of correlations between various variables discussed in the text was assessed using the p -value, whereby a value of ≤ 0.05 is taken to indicate statistical significance (i.e., the null hypothesis of no significant correlation is rejected); the corresponding results along with Pearson correlation coefficients r and number of observations are reported in Table 2. All statistical assessment was carried out using Microsoft Excel software. No Bayesian analysis or hierarchical and complex designs were performed.

Rationale and parameters for trace-element modelling. Model inputs and outputs described below are presented in Supplementary Tables 1–5.

Parental melt composition (C_0). To model V concentrations in crystals accumulated from a melt, an estimate for the parental melt composition is needed. The partitioning of V between olivine, the pyroxenes, spinel and melt as a function of temperature and oxygen fugacity has been parameterised by ref. ³⁵ to predict concentrations in peridotite-derived partial melts at different melt fractions. We use their spreadsheet to find V abundances in the melt at conditions specified in Supplementary Table 1. Wang et al.³⁵ employ a Depleted Mantle starting concentration of 73 ppm, which is adopted, consistent with findings that the mantle source of the protoliths to eclogite xenoliths was depleted (if heterogeneous) by ca. 3.0 Ga ago³⁶, the age of the oldest suite. The Mesoarchean ambient convecting mantle, from which the oceanic crustal protoliths of the majority of eclogite xenoliths were formed^{7,17}, was more reducing than today by 1–2 log units^{14,15,39} and hotter by some controversial amount^{36,37,58}. Here, we assume an Archaean mantle potential temperature T_p of ~ 1450 °C, some 150 °C hotter than today³⁶. These conditions imply higher melt fractions than today⁵⁹ and also have an effect on bulk distribution coefficients during peridotite melting³⁵. For an assumed melt fraction of 0.2 (ref. ³⁶) and $\Delta \log fO_2(\text{FMQ})$ of -2 , the peridotite-derived aggregated partial melt would contain ~ 170 ppm V; the same melt would

contain ~ 300 ppm V for $fO_2 = \text{FMQ}$ (Supplementary Table 1). For comparison, a parental melt formed at a fraction of 0.08, $fO_2 = \text{FMQ}$ and T_p of 1300 °C, taken to be representative of conditions of modern MORB formation, would contain ~ 210 ppm V. The parental MORB V estimate is lower than that of modern average NMORB (280 ppm) because the latter represents a differentiated magma with 7.8 wt.% MgO⁶⁰.

Low-pressure accumulation. We estimate the expected concentrations of V in a spinel-olivine-plagioclase cumulate for batch crystallisation using the C_0 estimate of 170 ppm for $\Delta \log fO_2(\text{FMQ})$ of -2 and 300 ppm for $fO_2 = \text{FMQ}$ described in the previous section. The corresponding fO_2 and crystallisation temperature (1340 °C; converted from T_p of 1450 °C following ref. ⁵⁹) were entered into the spreadsheet of ref. ³⁵ (all other parameters were adopted from the spreadsheet; note that the parameterisation of $D(V)$ does not contain a pressure term), wherefrom the temperature- and fO_2 -dependent olivine- and spinel-melt D were retrieved. As there are no published fO_2 -dependent $D(V)$ values for plagioclase, the average olivine/plagioclase- $D(V) = 2.5$ ^{61–64} is used to estimate plagioclase- $D(V)$ from that of olivine. For simplicity, the cooling of the melt during progressive crystallisation is ignored. Accumulation of 1% spinel, 20% olivine and 28% plagioclase prior to the onset of clinopyroxene crystallisation is modelled, based on the results of thermodynamic modelling for fractional crystallisation of a picritic melt at FMQ and a pressure of 0.05 GPa (from Appendix 5 in ref. ⁵⁷, neglecting small differences in phase relations arising from differences in fO_2 (see example modelled in Appendix 5 of ref. ⁵⁷). The modelled cumulate has < 30 ppm V at all investigated conditions (Supplementary Table 2).

Low-pressure melt evolution. The effect of progressive fractionation of 1% spinel, 20% olivine and 28% plagioclase (assumed to be sequential for simplicity) on V abundances in the melt is modelled using the C_0 estimate of 170 ppm at FMQ-2, and alternatively of 300 ppm V at $fO_2 = \text{FMQ}$, D values derived as described above, and the fractional crystallisation equation. At the chosen crystallisation temperature of 1340 °C, V switches from behaving compatibly in clinopyroxene at FMQ-2 to mildly incompatibly at FMQ, whereas it is always compatible in spinel, and incompatible in olivine and plagioclase (Supplementary Table 3). A difference of ± 50 °C in T_p and corresponding crystallisation temperature is additionally explored for $fO_2 = \text{FMQ-2}$, illustrating that V becomes more incompatible with increasing temperature³⁵. Thus, if higher T_p is assumed for the Archaean, the fO_2 isopleths shown in Fig. 5 are shifted upward relative to the samples, implying even more reducing conditions for Archaean oceanic crust.

High-pressure partial melt extraction (metamorphism). Oceanic crust subducting in the Archaean plausibly lost a partial melt^{9,65,66}. This is modelled as melt extraction from a rutile-eclogite⁶⁷, using garnet-melt and clinopyroxene-melt D from ref. ⁶⁸ for REE. For V, rutile-melt D as a function of fO_2 was parameterised from ref. ²⁶, clinopyroxene-melt D as a function of fO_2 was parameterised from ref. ¹² and garnet-melt D was assumed to be identical to clinopyroxene-melt D based on results reported in ref. ¹². These coefficients were chosen because the distribution coefficients suggested by ref. ³⁵ for peridotite melting do not return realistic clinopyroxene-melt $D(V)$ for the clinopyroxene compositions and relatively low temperatures near the eclogite solidus. While ref. ⁶⁸ does report clinopyroxene- and garnet-melt $D(V)$, their experiments were carried out at estimated fO_2 near IW, which is lower than fO_2 estimates for most eclogite xenoliths. Following ref. ⁵⁷, the residue composition was calculated for weight fractions of 0.445 clinopyroxene, 0.55 garnet and 0.005 rutile at various fO_2 , using a V concentration of 170 ppm as an eclogite starting composition. Whereas V remains compatible in rutile at all conditions, it behaves compatibly in clinopyroxene and garnet up to FMQ-1, but mildly incompatibly at FMQ (Supplementary Table 4). These results are semi-quantitative in the absence of experimental constraints on the fO_2 -dependent partitioning of V between eclogite garnet, clinopyroxene and melt.

Metasomatic clinopyroxene addition. The V concentration in clinopyroxene added by kimberlite metasomatism²¹ is modelled for crystallisation temperatures of 1200 and 1100 °C as examples (i.e., > 200 – 300 °C hotter than the average residence temperature of eclogite xenoliths; Table 1), and using distribution coefficients parameterised by ref. ³⁵, as above. This assumes that the fO_2 -dependent clinopyroxene-melt partitioning also applies to carbonated silicate melts, such as kimberlites, for which redox-dependent V partitioning data are not yet available. Vanadium concentrations in kimberlites vary considerably (e.g., 96 ± 62 ppm for the Renard kimberlite, 149 ± 32 ppm for the Wemindji kimberlite, both in the Superior craton⁶⁶), and this is the range explored in the modelling. For kimberlite with 100–150 ppm V, $fO_2 = \text{FMQ}$ and crystallisation temperature of 1100 °C, the resulting clinopyroxene would have 350–530 ppm V, but only 180–280 ppm V if the temperature were 1200 °C for $fO_2 = \text{FMQ}$ and 100–150 ppm V if the temperature were 1200 °C for $fO_2 = \text{FMQ} + 1$.

Data availability

No new data were generated as part of this study. References for the data on which this study is based are provided in the Supplementary Information file Supplementary Data 1.

Received: 17 August 2021; Accepted: 16 March 2022;

Published online: 08 April 2022

References

- Stagno, V. Carbon, carbides, carbonates and carbonatitic melts in the Earth's interior. *J. Geol. Soc.* **176**, 375 (2019).
- Luth, R. W. & Stachel, T. The buffering capacity of lithospheric mantle: implications for diamond formation. *Contrib. Mineral. Petrol.* <https://doi.org/10.1007/s00410-014-1083-6> (2014).
- Smit, K. V., Stachel, T., Luth, R. W. & Stern, R. A. Evaluating mechanisms for eclogitic diamond growth: an example from Zimmi Neoproterozoic diamonds (West African craton). *Chem. Geol.* **520**, 21–32 (2019).
- Haggerty, S. E. Diamond genesis in a multiply-constrained model. *Nature* **320**, 34–37 (1986).
- Foley, S. F. A reappraisal of redox melting in the Earth's mantle as a function of tectonic setting and time. *J. Petrol.* **52**, 1363–1391 (2011).
- Jacob, D. E. Nature and origin of eclogite xenoliths from kimberlites. *Lithos* **77**, 295–316 (2004).
- Shirey, S. B. & Richardson, S. H. Start of the Wilson cycle at 3 Ga shown by diamonds from subcontinental mantle. *Science* **333**, 434–436 (2011).
- Dawson, J. B. In *Kimberlites II: The mantle and crust-mantle relationships* (ed. J. Kornprobst) 282–331 (Elsevier, 1984).
- Ireland, T. R., Rudnick, R. L. & Spetsius, Z. Trace elements in diamond inclusions from eclogites reveal link to Archean granites. *Earth Planet. Sci. Lett.* **128**, 199–213 (1994).
- Stachel, T. & Luth, R. W. Diamond formation—where, when and how? *Lithos* **220**, 200–220 (2015).
- Canil, D. Vanadium partitioning between orthopyroxene, spinel and silicate melt and the redox states of mantle source regions for primary magmas. *Geochim. Cosmochim. Acta* **63**, 557–572 (1999).
- Mallmann, G. & O'Neill, H. S. C. The crystal/melt partitioning of V during mantle melting as a function of oxygen fugacity compared with some other elements (Al, P, Ca, Sc, Ti, Cr, Fe, Ga, Y, Zr and Nb). *J. Petrol.* **50**, 1765–1794 (2009).
- Lee, C. T. A., Leeman, W. P., Canil, D. & Li, Z. X. A. Similar V/Sc systematics in MORB and arc basalts: implications for the oxygen fugacities of their mantle source regions. *J. Petrol.* **46**, 2313–2336 (2005).
- Aulbach, S. et al. Evidence for a dominantly reducing Archean ambient mantle from two redox proxies, and low oxygen fugacity of deeply subducted oceanic crust. *Sci. Rep.* **9**, 20190 (2019).
- Nicklas, R. W. et al. Secular mantle oxidation across the Archean-Proterozoic boundary: evidence from V partitioning in komatiites and picrites. *Geochim. Cosmochim. Acta* **250**, 49–75 (2019).
- Stachel, T. & Harris, J. W. The origin of cratonic diamonds—Constraints from mineral inclusions: the Genesis of Gem Deposits. *Ore Geol. Rev.* **34**, 5–32 (2008).
- Gurney, J. J., Helmstaedt, H. H., Richardson, S. H. & Shirey, S. B. Diamonds through time. *Econ. Geol.* **105**, 689–712 (2010).
- Shirey, S. B. et al. Diamonds and the Geology of Mantle Carbon. *Carbon Earth* **75**, 355–4212 (2013).
- Aulbach, S., Heaman, L. M., Jacob, D. E. & Viljoen, K. S. Ages and sources of mantle eclogites: ID-TIMS and in situ MC-ICPMS Pb-Sr isotope systematics of clinopyroxene. *Chem. Geol.* **503**, 15–28 (2019).
- Helmstaedt, H. H. & Schulze, D. J. In *Kimberlites and Related Rocks. Proc. IV Kimberlite Conf. (Perth 1986)* Vol. 14 (ed. Ross, J.) 358–368 (Geological Society of Australia Special Publication, 1989).
- Aulbach, S. et al. Ultramafic carbonated melt- and auto-metasomatism in mantle eclogites: compositional effects and geophysical consequences. *Geochem. Geophys. Geosyst.* **21**, e2019GC008774 (2020).
- Smart, K. A. et al. The origin of high-MgO diamond eclogites from the Jericho Kimberlite, Canada. *Earth Planet. Sci. Lett.* **284**, 527–537 (2009).
- Gress, M. U., Pearson, D. G., Chinn, I., Thomassot, E. & Davies, G. R. Mesozoic to Paleoproterozoic diamond growth beneath Botswana recorded by ReOs ages from individual eclogitic and websteritic inclusions. *Lithos* <https://doi.org/10.1016/j.lithos.2021.106058> (2021).
- Timmerman, S., Koornneef, J. M., Chinn, I. L. & Davies, G. R. Dated eclogitic diamond growth zones reveal variable recycling of crustal carbon through time. *Earth Planet. Sci. Lett.* **463**, 178–188 (2017).
- Aulbach, S. Temperature-dependent rutile solubility in garnet and clinopyroxene from mantle eclogite: implications for continental crust formation and V-based oxybarometry. *J. Petrol.* **61**, ega065 (2020).
- Holycross, M. & Cottrell, E. Partitioning of V and 19 other trace elements between rutile and silicate melt as a function of oxygen fugacity and melt composition: implications for subduction zones. *Am. Mineral.* **105**, 244–254 (2020).
- Harte, B. & Kirkley, M. B. Partitioning of trace elements between clinopyroxene and garnet: data from mantle eclogites. *Chem. Geol.* **136**, 1–24 (1997).
- Papike, J. J. et al. Chromium, vanadium, and titanium valence systematics in Solar System pyroxene as a recorder of oxygen fugacity, planetary provenance, and processes. *Am. Mineral.* **101**, 907–918 (2016).
- Righter, K. et al. The effect of f(O₂) on the partitioning and valence of V and Cr in garnet/melt pairs and the relation to terrestrial mantle V and Cr content. *Am. Mineral.* **96**, 1278–1290 (2011).
- Shannon, R. D. Revised effective ionic-radii and systematic studies of interatomic distances in halides and chalcogenides. *Acta Crystallogr. Sect. A* **32**, 751–767 (1976).
- Sutton, S. R. et al. Vanadium K edge XANES of synthetic and natural basaltic glasses and application to microscale oxygen barometry. *Geochim. Cosmochim. Acta* **69**, 2333–2348 (2005).
- Liu, L., Xiao, Y., Aulbach, S., Li, D. & Hou, Z. Vanadium and niobium behavior in rutile as a function of oxygen fugacity: evidence from natural samples. *Contrib. Mineral. Petrol.* **167**, 1026 (2014).
- Locock, A., Luth, R. W., Cavell, R. G., Smith, D. G. W. & Duke, M. J. M. Spectroscopy of the cation distribution in the schorlomite species of garnet. *Am. Mineral.* **80**, 27–38 (1995).
- Stachel, T., Aulbach, S. & Harris, J. W. *Mineral Inclusions in Lithospheric Diamonds* (The Mineralogical Society of America, 2022).
- Wang, J. T. et al. Oxidation state of arc mantle revealed by partitioning of V, Sc, and Ti between mantle minerals and basaltic melts. *J. Geophys. Res. Solid Earth* **124**, 4617–4638 (2019).
- Aulbach, S. & Arndt, N. T. Eclogites as palaeodynamic archives: evidence for warm (not hot) and depleted (but heterogeneous) Archean ambient mantle. *Earth Planet. Sci. Lett.* **505**, 162–172 (2019).
- Ganne, J. & Feng, X. J. Primary magmas and mantle temperatures through time. *Geochem. Geophys. Geosyst.* **18**, 872–888 (2017).
- Sanfilippo, A., Tribuzio, R., Tiepolo, M. & Berno, D. Reactive flow as dominant evolution process in the lowermost oceanic crust: evidence from olivine of the Pineto ophiolite (Corsica). *Contrib. Mineral. Petrol.* <https://doi.org/10.1007/s00410-015-1194-8> (2015).
- Nicklas, R. W., Puchtel, I. S. & Ash, R. D. Redox state of the Archean mantle: evidence from V partitioning in 3.5–2.4 Ga komatiites. *Geochim. Cosmochim. Acta* **222**, 447–466 (2018).
- Woodland, A. B. & Koch, M. Variation in oxygen fugacity with depth in the upper mantle beneath the Kaapvaal craton, Southern Africa. *Earth Planet. Sci. Lett.* **214**, 295–310 (2003).
- Yaxley, G. M., Berry, A. J., Rosenthal, A., Woodland, A. B. & Paterson, D. Redox preconditioning deep cratonic lithosphere for kimberlite genesis—evidence from the central Slave Craton. *Sci. Rep.* **7**, 30 (2017).
- Creighton, S., Stachel, T., Eichenberg, D. & Luth, R. W. Oxidation state of the lithospheric mantle beneath Diavik diamond mine, central Slave craton, NWT, Canada. *Contrib. Mineral. Petrol.* **159**, 645–657 (2010).
- Aulbach, S., Sun, J., Tappe, S., Höfer, H. E. & Gerdes, A. Volatile-rich metasomatism in the cratonic mantle beneath SW Greenland: link to Kimberlites and mid-lithospheric discontinuities. *J. Petrol.* **58**, 2311–2338 (2017).
- Litasov, K. & Ohtani, E. The solidus of carbonated eclogite in the system CaO-Al₂O₃-MgO-SiO₂-Na₂O-CO₂ to 32 GPa and carbonatite liquid in the deep mantle. *Earth Planet. Sci. Lett.* **295**, 115–126 (2010).
- Litasov, K. D., Shatskiy, A. & Ohtani, E. Melting and subsolidus phase relations in peridotite and eclogite systems with reduced C-O-H fluid at 3–16 GPa. *Earth Planet. Sci. Lett.* **391**, 87–99 (2014).
- Heaman, L. M., Creaser, R. A. & Cookenboo, H. O. Extreme enrichment of high field strength elements in Jericho eclogite xenoliths: a cryptic record of Paleoproterozoic subduction, partial melting, and metasomatism beneath the Slave craton, Canada. *Geology* **30**, 507–510 (2002).
- Dawson, J. B. & Smith, J. V. MARID (mica-amphibole-rutile-ilmenite-diopside) suite of xenoliths in kimberlite. *Geochim. Cosmochim. Acta* **41**, 309–323 (1977).
- Giuliani, A. et al. The final stages of kimberlite petrogenesis: Petrography, mineral chemistry, melt inclusions and Sr-C-O isotope geochemistry of the Bultfontein kimberlite (Kimberley, South Africa). *Chem. Geol.* **455**, 342–356 (2017).
- Rudnick, R. L., McDonough, W. F. & Chappell, B. W. Carbonatite metasomatism in the northern Tanzanian mantle—petrographic and geochemical characteristics. *Earth Planet. Sci. Lett.* **114**, 463–475 (1993).
- Smart, K. A. et al. Eclogite formation beneath the northern Slave craton constrained by diamond inclusions: Oceanic lithosphere origin without a crustal signature. *Earth Planet. Sci. Lett.* **319**, 165–177 (2012).
- Krogh, E. J. The garnet-clinopyroxene Fe-Mg geothermometer—a reinterpretation of existing experimental data. *Contrib. Mineral. Petrol.* **99**, 44–48 (1988).
- Smit, K. V. et al. Origin of eclogite and pyroxenite xenoliths from the Victor kimberlite, Canada, and implications for Superior craton formation. *Geochim. Cosmochim. Acta* **125**, 308–337 (2014).
- Motsamai, T., Harris, J. W., Stachel, T., Pearson, D. G. & Armstrong, J. Mineral inclusions in diamonds from Karowe Mine, Botswana: super-deep sources for super-sized diamonds? *Mineral. Petrol.* **112**, 169–180 (2018).

54. Antweiler, R. C. Evaluation of statistical treatments of left-censored environmental data using coincident uncensored data sets. II. Group comparisons. *Environ. Sci. Technol.* **49**, 13439–13446 (2015).
55. Stachel, T. et al. The Victor Mine (Superior Craton, Canada): neoproterozoic lherzolitic diamonds from a thermally-modified cratonic root. *Mineral. Petrol.* **112**, 325–336 (2018).
56. Donovan, J. J., Lowers, H. A. & Rusk, B. G. Improved electron probe microanalysis of trace elements in quartz. *Am. Mineral.* **96**, 274–282 (2011).
57. Aulbach, S. & Jacob, D. E. Major- and trace-elements in cratonic mantle eclogites and pyroxenites reveal heterogeneous sources and metamorphic processing of low-pressure protoliths. *Lithos* **262**, 586–605 (2016).
58. Herzberg, C., Condie, K. & Korenaga, J. Thermal history of the Earth and its petrological expression. *Earth Planet. Sci. Lett.* **292**, 79–88 (2010).
59. Herzberg, C. & Asimow, P. D. Petrology of some oceanic island basalts: PRIMELT2.XLS software for primary magma calculation. *Geochem. Geophys. Geosyst.* <https://doi.org/10.1029/2008gc002057> (2008).
60. Gale, A., Laubier, M., Escrig, S. & Langmuir, C. H. Constraints on melting processes and plume-ridge interaction from comprehensive study of the FAMOUS and North Famous segments, Mid-Atlantic Ridge. *Earth Planet. Sci. Lett.* **365**, 209–220 (2013).
61. Aigner-Torres, M., Blundy, J., Ulmer, P. & Pettke, T. Laser Ablation ICPMS study of trace element partitioning between plagioclase and basaltic melts: an experimental approach. *Contrib. Mineral. Petrol.* **153**, 647–667 (2007).
62. Bindeman, I. N., Davis, A. M. & Drake, M. J. Ion microprobe study of plagioclase-basalt partition experiments at natural concentration levels of trace elements. *Geochim. Cosmochim. Acta* **62**, 1175–1193 (1998).
63. Laubier, M., Grove, T. L. & Langmuir, C. H. Trace element mineral/melt partitioning for basaltic and basaltic andesitic melts: an experimental and laser ICP-MS study with application to the oxidation state of mantle source regions. *Earth Planet. Sci. Lett.* **392**, 265–278 (2014).
64. Norman, M., Garcia, M. O. & Pietruszka, A. J. Trace-element distribution coefficients for pyroxenes, plagioclase, and olivine in evolved tholeiites from the 1955 eruption of Kilauea Volcano, Hawai'i, and petrogenesis of differentiated rift-zone lavas. *Am. Mineral.* **90**, 888–899 (2005).
65. Smart, K. A., Chacko, T., Simonetti, A., Sharp, Z. D. & Heaman, L. M. A record of paleoproterozoic subduction preserved in the Northern Slave Cratonic Mantle: Sr-Pb-O isotope and trace-element investigations of eclogite xenoliths from the Jericho and Muskox Kimberlites. *J. Petrol.* **55**, 549–583 (2014).
66. Tappe, S. et al. Plates or plumes in the origin of kimberlites: U/Pb perovskite and Sr-Nd-Hf-Os-C-O isotope constraints from the Superior craton (Canada). *Chem. Geol.* **455**, 57–83 (2017).
67. Rapp, R. P., Shimizu, N. & Norman, M. D. Growth of early continental crust by partial melting of eclogite. *Nature* **425**, 605–609 (2003).
68. Barth, M. G., Foley, S. F. & Horn, I. Partial melting in Archean subduction zones: constraints from experimentally determined trace element partition coefficients between eclogitic minerals and tonalitic melts under upper mantle conditions. *Precambrian Res.* **113**, 323–340 (2002).
69. Sun, S.-S. & McDonough, W. F. In *Magmatism in the Ocean Basins* (eds. A. D. Saunders & M. J. Norry) 313–345 (Geological Society, 1989).
70. Stagno, V., Frost, D. J., McCammon, C. A., Mohseni, H. & Fei, Y. The oxygen fugacity at which graphite or diamond forms from carbonate-bearing melts in eclogitic rocks. *Contrib. Mineral. Petrol.* <https://doi.org/10.1007/s00410-015-1111-1> (2015).
71. Jenner, F. E. & O'Neill, H. S. Analysis of 60 elements in 616 ocean floor basaltic glasses. *Geochem. Geophys. Geosyst.* **13**, Q02005 (2012).
72. O'Neill, H. S., Berry, A. J. & Mallmann, G. The oxidation state of iron in Mid-Ocean Ridge Basaltic (MORB) glasses: Implications for their petrogenesis and oxygen fugacities. *Earth Planet. Sci. Lett.* **504**, 152–162 (2018).

Acknowledgements

Andrew Locock at University of Alberta is thanked for discussion of sources of error when determining V abundances by electron probe microanalyser (EPMA), and Dominik Hezel at Goethe-University Frankfurt for his help with testing the accuracy of V₂O₃ determination by EPMA. The Deutsche Forschungsgemeinschaft is gratefully acknowledged for funding to S.A. (DFG-grant # AU356/11).

Author contributions

S.A. conceived the study, collated xenolith data and wrote the first draft of the manuscript. T.S. collated the DI data and contributed to discussion and manuscript revision.

Funding

Open Access funding enabled and organized by Projekt DEAL.

Competing interests

The authors declare no competing interests.

Additional information


Supplementary information The online version contains supplementary material available at <https://doi.org/10.1038/s41467-022-29567-z>.

Correspondence and requests for materials should be addressed to Sonja Aulbach.

Peer review information *Nature Communications* thanks Willie Nicklas and the other, anonymous reviewer(s) for their contribution to the peer review of this work. Peer reviewer reports are available.

Reprints and permission information is available at <http://www.nature.com/reprints>

Publisher's note Springer Nature remains neutral with regard to jurisdictional claims in published maps and institutional affiliations.

 **Open Access** This article is licensed under a Creative Commons Attribution 4.0 International License, which permits use, sharing, adaptation, distribution and reproduction in any medium or format, as long as you give appropriate credit to the original author(s) and the source, provide a link to the Creative Commons license, and indicate if changes were made. The images or other third party material in this article are included in the article's Creative Commons license, unless indicated otherwise in a credit line to the material. If material is not included in the article's Creative Commons license and your intended use is not permitted by statutory regulation or exceeds the permitted use, you will need to obtain permission directly from the copyright holder. To view a copy of this license, visit <http://creativecommons.org/licenses/by/4.0/>.

© The Author(s) 2022